

Journal of Materials Chemistry A

Accepted Manuscript



This is an *Accepted Manuscript*, which has been through the Royal Society of Chemistry peer review process and has been accepted for publication.

Accepted Manuscripts are published online shortly after acceptance, before technical editing, formatting and proof reading. Using this free service, authors can make their results available to the community, in citable form, before we publish the edited article. We will replace this *Accepted Manuscript* with the edited and formatted *Advance Article* as soon as it is available.

You can find more information about *Accepted Manuscripts* in the [Information for Authors](#).

Please note that technical editing may introduce minor changes to the text and/or graphics, which may alter content. The journal's standard [Terms & Conditions](#) and the [Ethical guidelines](#) still apply. In no event shall the Royal Society of Chemistry be held responsible for any errors or omissions in this *Accepted Manuscript* or any consequences arising from the use of any information it contains.

Highly dispersion of TiO₂ nanocrystals within porous carbon towards tunable lithium storage ability and its battery application versus LiNi_{0.5}Mn_{1.5}O₄

Cite this: DOI: 10.1039/x0xx00000x

Hai Ming,^{a,b} Jun Ming,^{*b} Seung-Min Oh,^b Eung-Ju Lee,^b Hui Huang,^c Qun Zhou,^a Junwei Zheng,^{*a} and Yang-Kook Sun^{*b}

Received 00th January 2012,
Accepted 00th January 2012

DOI: 10.1039/x0xx00000x

www.rsc.org/

A new and simple strategy was developed to well disperse TiO₂ nanocrystals into the porous carbon (i.e., PC), and a series of hierarchical PC-TiO₂ composite with different architectural structures were synthesized. Varying the amount of TiO₂, the lithium storage capacity of PC-TiO₂ (from 30 wt% TiO₂ to 64 wt%) could be controlled from 546 mAh g⁻¹ to 446 mAh g⁻¹ under the current density of 50 mA g⁻¹. And also, a very stable cycling performances and rate capabilities could also be obtained at the rate of 50 mA g⁻¹ to 1600 mA g⁻¹. Further increasing the content of TiO₂ to 93%, another new composite of TiO₂-C was also prepared and it demonstrated a high capacity of 352 mAh g⁻¹ at 50 mA g⁻¹, which was much higher than most reported TiO₂ materials. Based on above results, new full cells versus cathode of LiNi_{0.5}Mn_{1.5}O₄, such as PC-TiO₂/LiNi_{0.5}Mn_{1.5}O₄, was successfully assembled and investigated. This full cell not only delivered a high energy density of 413 Wh kg⁻¹ but also showed good rate capability and an energy retention of 90.5% over 100 cycles.

Introduction

Designing one kind of material with advanced structure is of great interest because they can endow materials with superior properties in their applications. For example, the materials with specific structures, such as particles (e.g., core-shell structured Pt@mSiO₂,¹ C@Ni,² hollow TiO₂),³ tubes (e.g., Fe₂O₃/CNTs,⁴ La_{0.75}Sr_{0.25}MnO₃ nanotube⁵), and hierarchical materials (e.g., porous Cu-SnO₂,⁶ ZnO-ZrO₂,⁷ SnO₂-C,⁸ porous carbon-CoO_x,⁹ Co_xMn_{3-x}O₄¹⁰), usually showed an improved performance than bulk one in catalysis, sensor, environmental and energy area. As well reported in many previous literatures,¹¹⁻²⁴ the anode of TiO₂ was a beneficial alternative of the graphite in the lithium ion battery for the electric vehicle/hybrid electric vehicle, because it could prevent the formation of lithium dendrites and be superior owing to its excellent rate and non-flammable properties. Prompting by the high performance resulted from the unique compositions and/or structures as demonstrated, herein we introduced an intriguing kind of hierarchical materials mainly consisting of porous carbon matrix, in which ultra-small TiO₂ nanocrystals (< 5 nm) was highly dispersed, and it possessed a tunable lithium storage ability in lithium-ion battery application.

To date, numerous nano-structured TiO₂ materials with fantastic morphologies, such as solid/hollow particles,¹¹⁻¹⁵ wires,¹⁶⁻¹⁸ tubes,¹⁹⁻²¹ and arrays,²²⁻²⁴ have been prepared and

indeed they exhibited excellent performance in lithium ion battery application. However, considering the viewpoint of future industrial application, it would be significant to develop one method to synthesize them in a large scalable production. And also, pursuing a hierarchical structure near the size of micro-meter was preferred for the easy process,¹³ meanwhile maintaining nanostructure of TiO₂ should also be carefully controlled. Unfortunately, the nanostructured TiO₂ still always gave rise to a low electronic transferability due to the physical interconnection between the binder (e.g., polyvinylidene fluoride, PVDF) and conductive carbon (e.g., Super P or acetylene black) in the electrode.^{18, 25} Therefore, disperse the TiO₂ nanocrystals into the matrix of porous carbon in advance could largely improve the conductivity/connectivity of TiO₂ due to the close contact of carbon and TiO₂, and also it could ingress the electrolyte into the structure *via* the pores to promise the high rate capability. Particularly, the carbon with a capacity arranging from 372 to 1200 mAh g⁻¹ or more could also largely increase the capacity of composite,²⁶ because the pure TiO₂ (Rutile, Anatase, Brookite) often delivered a limited capacity between 168~316 mAh g⁻¹ *via* up/take of 0.5~1.0 Li⁺.^{27, 28} Moreover, the stable physicochemical properties of carbon could also enhance the cycling ability through protecting TiO₂ nanocrystals from any aggregation or collapse. Besides, the typical high discharge/charge voltage of TiO₂ around 1.7 V (vs. Li⁺/Li) could also be reduced to a lower value after introducing

the carbon, and then a higher energy density in a full battery could be achieved.

It is interesting to apply TiO₂ particles as small as several nano meters in Li-ion batteries, because it can: (i) maintain the intriguing properties of nanomaterials and also decrease the pathway of lithium ions during insertion/extraction to promise a high rate performance; (ii) largely reduce the strain tension of materials to keep the cycling performance; (iii) increase the ratio of surface to volume and then get a large contact area between TiO₂ and the electrolyte, then making a high utilization of active materials with an improved capacity. Although the researches about preparing the composite of TiO₂ and carbon, such as porous TiO₂/C,²⁹⁻³² TiO₂/C composite nanorods,³³ CNTs@TiO₂,³⁴ sandwich-like TiO₂@C,³⁵ and TiO₂/C composite tubes,³⁶ have been reported before, a try of dispersing TiO₂ nanocrystals into the porous carbon uniformly was rarely to be achieved, let alone processed in a large scalable and simple approach.

Even the TiO₂ and TiO₂-based materials have been always prepared and utilized as anode in the lithium-ion battery, most of their properties were only tested in the half-cell versus the electrode of lithium metal. Actually, it is quite necessary to investigate them in a full cell, because it could evaluate the performance more accurately as that in practical application. To date, only few literature concerning using the pure TiO₂ materials as anode versus the cathode of LiFePO₄ and LiNi_{0.5}Mn_{1.5}O₄ for a full battery.¹⁶ However, as mentioned before, the low capacity of TiO₂ near 168 mAh g⁻¹ need to be further enhanced while the voltage around 1.7 V deserve to be reduced for getting a higher energy density (Wh kg⁻¹, which was calculated by the integral of discharge curve in the curve of voltage-capacity).

Stimulating by these reasons, we successfully dispersed the ultra-small TiO₂ nanocrystals (1-5 nm) into the porous carbon *via* the way of *in-situ* thermal decomposition of tetrabutyl titanate (TBT) in the resin, which could be readily expanded to prepare other kind of PC-metal (oxide) composite just varying the kind of precursor. Benefiting the convenient of this method, the amount of TiO₂ was finely controlled and its effect to the final lithium storage ability was discussed in detail. Moreover, new full batteries versus high voltage cathode of LiNi_{0.5}Mn_{1.5}O₄ were configured and the electrochemical properties with using different kind of anodes (*e.g.*, PC-TiO₂, 30wt%; TiO₂-C, 93wt%) were systematically investigated. Promisingly, for example, the battery of PC-TiO₂/LiNi_{0.5}Mn_{1.5}O₄ could deliver a high energy density of 413 Wh kg⁻¹ and also show good rate capability with an energy retention of 90.5% after 100 cycles.

Experimental

Materials synthesis

In a typical synthesis, 5 mL phenolic resin's ethanol solution (0.25 g mL⁻¹) and 3 g F127 were dissolved into 50 mL ethanol solution firstly, and then adding 2.5 mL tetrabutyl titanate (TBT) into solution give rise to a yellow sol-gel. Further dry the yellow intermediate at 70 °C for 24 h and then calcine at 600 °C

under the N₂ atmosphere for 4 hours. In this experiment, the resin was a carbon precursor and triblock copolymer F127 acted as a porous structural template for the pores formation.³⁷ During the thermal treatment and calcination, the highly dispersed TBT will form highly dispersed TiO₂ nanocrystals, which would be coated by the layer of porous carbon due to the carbonization of resin and F127. Finally, the product of PC-TiO₂ was obtained. Increase the precursor of TBT to 5 and 10 mL, the amount of TiO₂ in the porous carbon was readily tuned. Besides, the TiO₂ with traces of carbon, abbreviated as TiO₂-C, was prepared under the calcination of yellow intermediates in air atmosphere, in which 10 mL TBT was used. Without adding the TBT, pure porous carbon was prepared under the same procedure. The TiO₂ nanoparticles were obtained based on the procedure as reported recently.¹⁵

Electrode preparation

The active materials of TiO₂-C and PC-TiO₂, conductive carbon of Super P, and the binder of PVDF with the mass ratio of 8:1:1 were mixed in the solution of N-methyl pyrrolidinone (NMP) to form a uniform slurry, which was then casted on the copper foil. After drying in a vacuum oven at 120 °C for 12 h, the foil was punched into circular sheets with a diameter of 14 mm (Ø14). The mass density of PC-TiO₂ was about 1.5 mg cm⁻². The cathode electrode consisting of LiNi_{0.5}Mn_{1.5}O₄ was also prepared in the same way. The mass density of LiNi_{0.5}Mn_{1.5}O₄ was about 4.5 and 6.0 mg cm⁻². The electrochemical test was carried out with 2032-type coin cell, in which using lithium metal as the counter electrode. The cell was assembled in a glove box filled with pure argon, in which the content of moisture and oxygen were below 0.1 ppm. Microporous polypropylene film (Celgard2400) was used as the separator, and the electrolyte was 1.0 mol L⁻¹ LiPF₆ dissolved in a mixture of ethyl methyl carbonate (EMC) and ethylene carbonate (EC) in the weight ratio of 1:1. The configuration of full battery was based on the procedures as reported recently.³⁸

Characterization

The crystal information was characterized by the X-ray powder diffraction (XRD) using a X'Pert-ProMPD (Holand) D/max-γA X-ray diffractometer with Cu Kα radiation (λ = 0.154178 nm). Scanning electron microscopy (SEM) and EDX were taken on a FEI-quanta 200F scanning electron microscope with acceleration voltage of 30 kV. The distribution of TiO₂ nanocrystals in the carbon matrix was characterized by the transmission electron micrograph (TEM) with using the FEI-Tecna F20 (200 kV) transmission electron microscope (FEI). Nitrogen adsorption-desorption isotherms were obtained using the instrument of ASAP2050 (Micromeritics Instrument Corp.) surface area & porosity Analyzer at 77 K. The specific surface area was calculated by the Brunauer-Emmett-Teller (BET) method. Thermogravimetric analysis (TGA, NETZSCH, TG-209-F3) was carried out under a flow of air with a temperature ramp of 5 °C min⁻¹. All the electrochemical measurements were tested and recorded automatically by the instrument of TOCAST 3100 at the temperature of 30 °C. Cyclic

voltammetry (CV) within the voltages of 0.01-3.0 V and impedance analysis in the frequency ranging from 100 kHz and 10 mHz. were both performed using the VMP-3 instrument.

Results and Discussion

Materials characterization

With varying the precursor of TBT from 2.5, 5 to 10 mL, the mass percent of TiO₂ in the PC-TiO₂ composites increased from 30 wt%, 52 wt% to 64wt%, as confirmed by the TGA (Fig. 1). Alternatively, another composite of TiO₂-C containing 93wt% TiO₂ were obtained after calcination of yellow intermediate in air. The traces of carbon was always hard to burn completely at a relative low temperature (~ 600 °C) within a short time of several hours, and this phenomena was similar as reported as before.^{39, 40} According to the XRD patterns, the

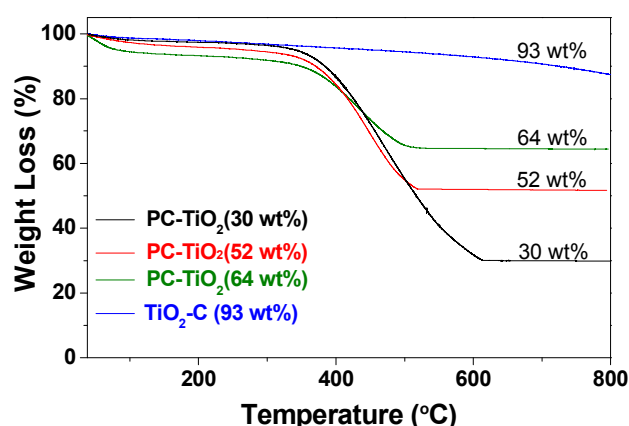


Fig. 1 TGA analysis of PC-TiO₂ and TiO₂-C with different loading of TiO₂ nanocrystals.

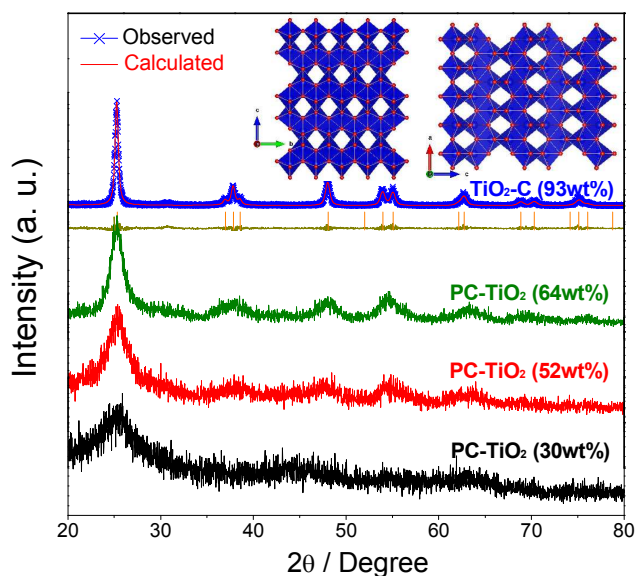


Fig. 2 XRD patterns of PC-TiO₂ with different mass percent of TiO₂ nanocrystals, and XRD and Rietveld refinement of TiO₂-C (93wt%). Inset image is a typical crystal graphical structure of TiO₂ with space group of I41/AMDS visually along the (100) and (010) direction.

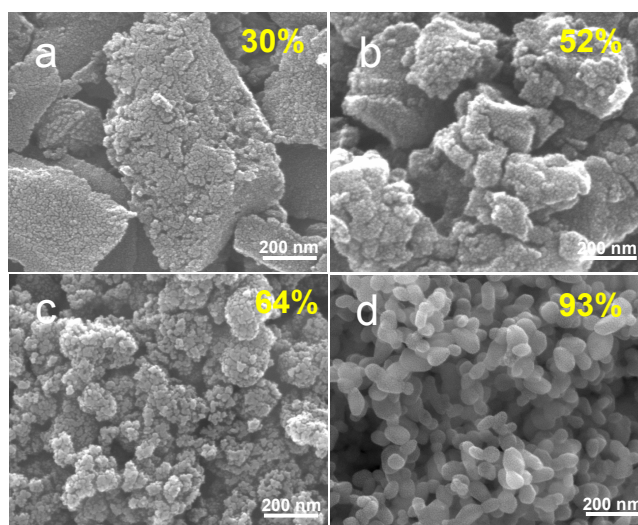


Fig. 3 SEM images of (a) PC-TiO₂ (30%), (b) PC-TiO₂ (52%), (c) PC-TiO₂ (64%) and (d) TiO₂-C (93%) with different loading of TiO₂ nanocrystals.

crystalline structure of TiO₂ in the PC-TiO₂ and TiO₂-C composite were all ascribed to the anatase TiO₂ (JCPDS Card No. 89-4319). The diffraction peaks of TiO₂ in the PC-TiO₂ composite became stronger and sharper gradually as increasing the amount of TiO₂. It is reasonable because the increased amount of TiO₂ and reduced barrier of carbon could facilitate the growth of oxide crystals during the calcination. Logically, the TiO₂-C with traces of carbon showed the highest degree of crystallization. Through the Rietveld refinement of TiO₂-C, the crystalline structure of TiO₂ has the unit parameters of $a=b=3.784(1)$ Å, $c=9.498(1)$ Å (Fig. 2). Such kind crystalline structure has two channels which could be available for the insertion/de-insertion of lithium ions along the (100) and (010) directions (Inset of Fig. 2). Moreover, the connected octahedral TiO₆ with edge-sharing was quite stable. Both two points well ensure their widespread applications in lithium ion batteries.

All the products of PC-TiO₂ have a hierarchical structure, in which the primary nanoparticles aggregated densely through the carbon layer, which could be clearly observed in the sample of PC-TiO₂ (30wt%) (Fig. 3a). With increasing the amount of TiO₂, the particle size of PC-TiO₂ become smaller due to the limitation of connected carbon (Fig. 3a-c). While for the sample of TiO₂-C (93wt%), it consist of connected TiO₂-C nanoparticles around the size of 100 nm, forming the micro-sized hierarchical structure like a coral (Fig. 3d).

With further characterized by the TEM, we could observe that numerous ultra-uniform TiO₂ nanocrystals were embedded in the skeleton structure of porous carbon with a high distribution. For the material of PC-TiO₂ (30wt%), the size distribution of TiO₂ was about 1-5 nm, and the average value was about 3 nm, as confirmed by the black crystalline dots in Fig. 4a-b. The amorphous shadow and bright blank area under TEM correspond to the connected carbon matrix and porosity, respectively. As demonstrated in HRTEM (Fig. 3c), the TiO₂ nanocrystals have the characteristic of polycrystalline, as confirmed by the interlaced crystalline boundaries and FFT

pattern (insert in Fig. 3c). For the single TiO₂ nanocrystal, most areas showed the lattice fringes with a spacing of 0.35 nm that corresponding to the (101) planes of TiO₂ (Fig. 4c), which were well accordance with the XRD patterns. With increasing the amount of TiO₂, the size of nanocrystals increased to 6 nm for the sample of PC-TiO₂ (64wt%) (Fig. 4d). While for the TiO₂-C (93 wt%), a serious aggregation of TiO₂ nanoparticles could be well observed (Fig. 4e), and it seems that they were surrounded by little part of carbon (Fig. 4f), as judged from the amorphous layer on the surface of the particles.

The rich porosity in the structure of PC-TiO₂ composite was also characterized by the N₂ adsorption-desorption isotherms (Fig. 5). The samples of PC-TiO₂ exhibited a typical type-IV isotherm,⁴¹ demonstrating the porous characteristic of the

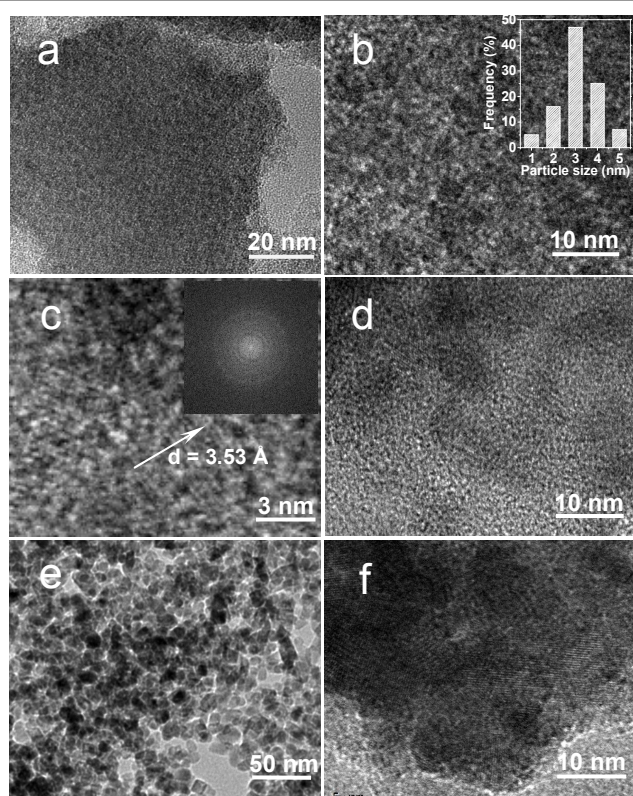


Fig. 4 (a) SEM, (b) TEM, (c) HRTEM images of PC-TiO₂ (30 wt%). Inset of (b) and (c) is the size distribution and FFT pattern of TiO₂ nanocrystals respectively. (d) Typical HRTEM image of PC-TiO₂ (64 wt%). (e) TEM and (f) HRTEM image of TiO₂-C (93wt%) composite.

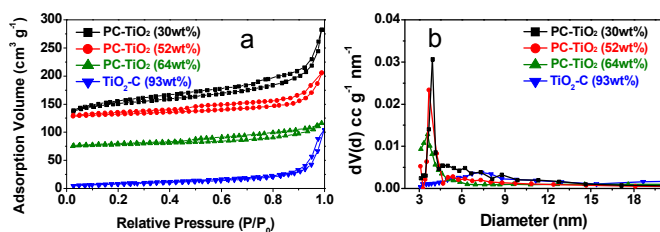


Fig. 5 (a) Comparative analysis of N₂ adsorption-desorption isotherms and (b) pore size distributions of PC-TiO₂ and TiO₂-C.

Table 1 Physical characteristic of PC-TiO₂ and TiO₂-C composite.

Kind of sample	Surface area / m ² g ⁻¹	Pore volume / cc g ⁻¹	Pore size / nm
PC-TiO ₂ (30wt%)	409	0.86	3.9
PC-TiO ₂ (52wt%)	303	0.67	3.7
PC-TiO ₂ (64wt%)	169	0.35	3.7
TiO ₂ -C(93wt%)	29	0.08	7.7

composite, which were the same as observed under TEM (Fig 4b). But this feature was not obvious for the TiO₂-C composite due to the aggregation. The BET specific surface of the PC-TiO₂ (30wt%, 52wt%, 64wt%) were about 409, 303, and 169 m² g⁻¹ respectively, which were larger than that of TiO₂-C (29 m² g⁻¹). The Barrett-Joyner-Halenda (BJH) plots revealed that the pore size distribution of PC-TiO₂ were mainly focused on 3.7-3.9 nm, which were smaller than that of TiO₂-C (7.7 nm) (Fig. 5b, Table 1). Increasing the mass percent of TiO₂ from 30wt%, 52wt%, 64wt% to 93wt%, the pore volume was decreased from 0.86, 0.67, 0.35 to 0.08 (Table 1), demonstrating the importance of carbon to preserve the porous structure. In brief, the results showed that a series of TiO₂-based materials, such as PC-TiO₂ and TiO₂-C, could be synthesized successfully *via* this simple sol-gel method. And also, the high surface area, rich pore volume and meso-porous characteristic of composite are available for the wide applications of photo-catalysis, solar cell and lithium-ion battery. Note that the conductivity of the porous carbon could achieve 4.95 S cm⁻¹, which were tested by the Advanced Instrument Technology (CMT-SR1000N).

Electrochemical performance versus lithium metal

The electrochemical performance of PC-TiO₂ and TiO₂-C in the LIBs were evaluated in the half-cell firstly, and comparative CV were presented in Fig. 6. For the TiO₂-C (93wt%), the sharp oxidation peak around 1.70 V in the anodic scan, and the reduction peak near 2.10 V in the cathodic scan, were well associated with the Ti⁴⁺/Ti³⁺ redox couple during lithium insertion/extraction. But these characteristic become weaker and then disappeared in the PC-TiO₂ composite with decreasing the TiO₂ to 30wt%. For example, the typical cathodic peak, corresponding to the discharge process, moved towards a higher value of 1.77 and 1.79 V. It demonstrate that the insertion of lithium ions into TiO₂ nanocrystals become easier than agglomerated TiO₂ particles in TiO₂-C. Inversely, the anodic peak, matching with the charge process, moved to a lower value of 2.07 and 2.01 V, confirming the easier extraction of lithium ions. Clearly, both results confirmed the easier insertion/extraction of lithium ions in TiO₂ nanocrystals. Moreover, the voltage difference between the anodic and cathodic peaks were also decreased from 0.4, 0.3 to 0.23 V for the samples of TiO₂-C (93wt%) and PC-TiO₂ (64wt%, 52wt%). It indicated that the PC-TiO₂ composite has a lower electrochemical polarization and a better reversibility during the discharge/charge process.

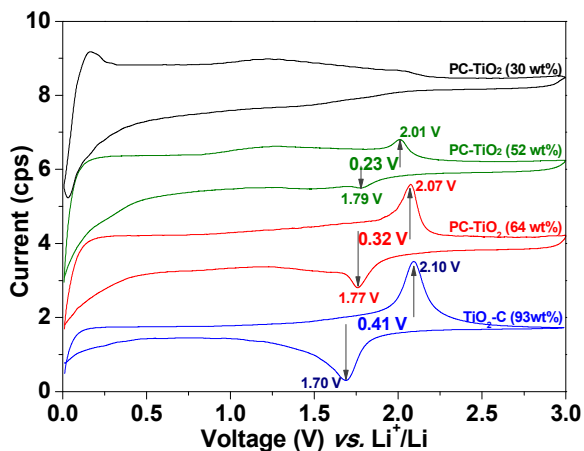


Fig. 6 Comparative cyclic voltammograms (CV) of PC-TiO₂ and TiO₂-C composite. Conditions, 0.1 mV s⁻¹, 0.01-3 V.

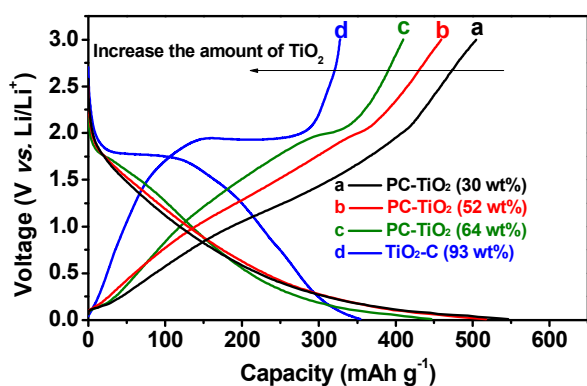


Fig. 7 Voltage profiles of PC-TiO₂ and TiO₂-C composite at the current density of 50 mA g⁻¹.

The charge/discharge voltage profiles were provided in Fig. 7, and they matched well with the CV analysis. For the sample of TiO₂-C (93wt%), a long plateau region of typical TiO₂ around 1.7 V existed and only a short tail below 1.7 V to 0.01 V (i. e., which correspond to the lithium storage in the porosity of material). While for the samples of PC-TiO₂, the voltage plateau region almost disappeared and moved toward a lower value below 1.7 V (Fig. 7). And also, the long plateau below 0.8 V emerged and it could be ascribed to the lithium insertion in carbon matrix and/or porosity of PC-TiO₂. As a result, a high capacity of 546, 517, 446 mAh g⁻¹ could be delivered by the samples of PC-TiO₂ (30 wt%, 52wt% and 64wt%) respectively. Noteworthy, the TiO₂-C composite with traces of carbon also demonstrated a high capacity of 352 mAh g⁻¹, which was much higher than those previously reported TiO₂ materials (e.g., 180-200 mAh g⁻¹).¹¹⁻²⁴ This interesting result need to be further investigated, and one part of the reason should be ascribed to the aggregated nanocrystals, traces of carbon, and/or porosity.

The rate capability of PC-TiO₂ and TiO₂-C composite were shown in Fig. 8a. Compared with TiO₂-C electrode, the PC-TiO₂ always exhibited a higher capacity at each rate due to the contribution of porous carbon and TiO₂ nanocrystals. The sample of PC-TiO₂ (30wt%) showed the highest capacities at the current density of 50 mA g⁻¹. In detail, it showed 544, 489,

394, 318, 277, 234 mAh g⁻¹ at the current density of 50, 100, 200, 400, 800, 1600 mA g⁻¹. Finally, it could recover back to 540 mAh g⁻¹ at 50 mA g⁻¹ after the end of rate test. With increasing the TiO₂ nanocrystals to 52wt% and 64wt%, the capacity changed to 515, 479, 421, 366, 316, 261 mAh g⁻¹, and 447, 414, 369, 318, 303, 285 mAh g⁻¹ under the same variation of current density. At the high rate test, the contribution of porous carbon was always limited, and then the rate capability properties of PC-TiO₂ (50wt%, 64 wt%) behavior little better than that of PC-TiO₂ (30wt%). While for the samples of TiO₂-C, it could deliver capacities of 352, 314, 285, 263, 232, 190 mAh g⁻¹ under the same trend of current density, and also it could recover back to the initial capacities under the 200 and 50 mA g⁻¹, as those of PC-TiO₂. Note that the performance of TiO₂-C behaviors better than most TiO₂ materials reported before,^{20, 42-45} particularly at the high rate.

More promisingly, the PC-TiO₂ and TiO₂-C composite both showed a very stable cycling ability. For example, an average capacity of 533, 501, 438, 348 mAh g⁻¹ could be obtained for the samples of PC-TiO₂ (30wt%, 52wt%, 64wt%) and TiO₂-C (93wt%) at 50 mA g⁻¹ over 80 cycles. Particularly, their capacity retention were as high as 98%, 95%, 101% and 100% (vs. the 3rd cycle) respectively. Increasing the current density to 1600 mA g⁻¹, the high capacities of 235, 260, 285 and 197 mAh g⁻¹ were also obtained in above samples, accompanying the capacities retention of 98%, 104%, 99% and 99%, successively. As mentioned before, the capacity contribution of carbon was limited at high rate, therefore the sample of PC-TiO₂ (30wt%) demonstrated a lowered capacity than those of PC-TiO₂ (52wt%) and PC-TiO₂ (64wt%) (Fig. 8b).

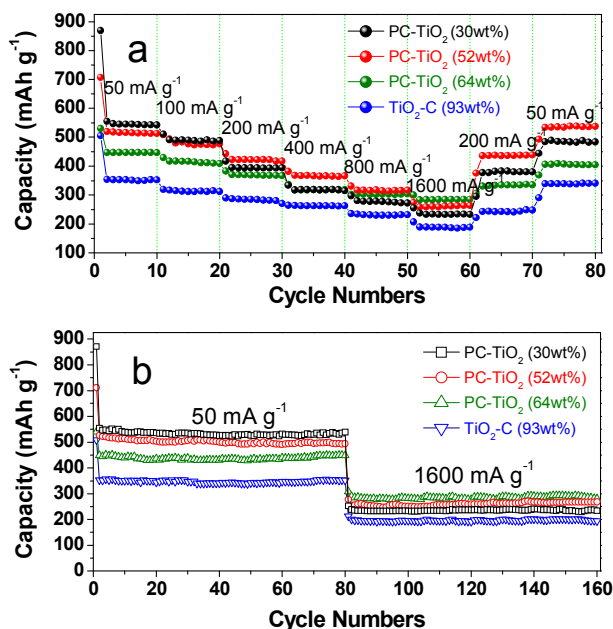


Fig. 8 (a) Rate capability of PC-TiO₂ and C-TiO₂ at different current densities (50-1600 mA g⁻¹). (b) Cycling performances of PC-TiO₂ and TiO₂-C at different current densities of 50 and 1600 mA g⁻¹.

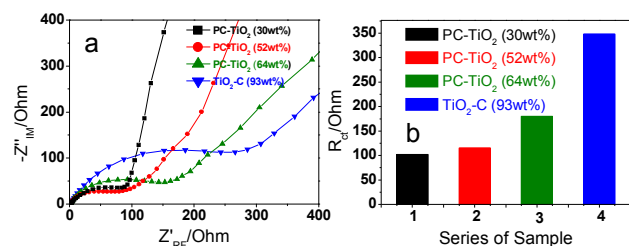


Fig. 9 (a) Nyquist impedance plots and (b) Comparative R_{ct} of lithium-ion coin-shape cell of PC-TiO₂ and TiO₂-C.

The high performance of PC-TiO₂, particularly the higher capacity compare to that of C-TiO₂, undoubtedly should be ascribed to the porous carbon. It could provide a capacity contribution, a protection and an enhancement of the conductivity for the dispersed TiO₂ nanocrystals, as further confirmed by the impedance analysis (Fig. 9a). The charge-transfer resistance (R_{ct}) of TiO₂-C was 348 Ω , as determined by the numerical value of width of semicircle on the Z' axis. It was much higher than 180 Ω of PC-TiO₂ (64wt%), 115 Ω of PC-TiO₂ (52wt%), 102 Ω of PC-TiO₂ (30wt%), fully demonstrating the higher electronic conductivity of PC-TiO₂. Moreover, a sharper tail of Nyquist plots in the low frequency of Fig. 9b also represented a higher diffusion of lithium ions in the electrode of PC-TiO₂ than that of TiO₂-C.⁴⁶ In brief, the higher electronic conductivity and lithium ion diffusion rate mainly resulted from the carbon matrix and high dispersion of TiO₂ nanocrystals, which are then responsible for the high performance of PC-TiO₂.

To make clear the advantage of PC-TiO₂ composite, the porous carbon and normal TiO₂ nanoparticles were further prepared respectively. Ball-milling the Super P or PC with TiO₂ nanoparticles in the mass ratio of 64%, giving rise to the composite of SP-TiO₂ (64 wt%, physically mixed) and PC-TiO₂ (64 wt%, physically mixed). We elevated these materials in the lithium ion batteries under the same conditions, and the comparative data were shown in the Fig. S1. Clearly, the capacity and the stability of PC-TiO₂ (64 wt%) were better than that of PC-TiO₂ (64 wt%, physically mixed), and the former two are better than SP-TiO₂ (64 wt%, physically mixed). It confirmed that the improvement of properties should be ascribed to the good dispersion of TiO₂ nanocrystals in the porous carbon and the well contact of TiO₂ and porous carbon. Individually, the pure PC has a capacity of 532 mAh g^{-1} with a poor cycling, while the TiO₂ nanoparticles has a low capacity of 183 mAh g^{-1} with a relative good stability (102%). While the composite of PC-TiO₂ (30wt%) has a higher capacity of 570 mAh g^{-1} , which is much better than that of pure PC and TiO₂ nanoparticles, well demonstrating the advantages of PC-TiO₂ composite.

Electrochemical performance versus LiNi_{0.5}Mn_{1.5}O₄

The electrochemical performance of PC-TiO₂ (30wt%) and TiO₂-C (93wt%) composite were also investigated in the full battery versus the LiNi_{0.5}Mn_{1.5}O₄. For the sample of PC-TiO₂ (30wt%), the coulombic efficiency (i.e., $CE =$

discharge/charge capacity) in the first cycle was 68% (i.e., 97 $\text{mAh g}^{-1}/143 \text{mAh g}^{-1}$), and it increased fast close to 98% following cycles (Fig. 10a, b). The reason of low CE in the first cycle should be ascribed to the defects of porous carbon which will consume lithium ions irreversibly, as well as the decomposition of electrolyte and forming the solid-electrolyte interface at the high charge voltage.⁴⁷⁻⁴⁹ In the initial 100 cycles, the cell demonstrated a good cycling performance with a capacity retention of 97.9% (vs. the 2nd cycle), accompanying a work voltage around 3.75 V and an average discharge capacity of 105 $\text{mAh g}_{\text{cathode}}^{-1}$. The energy density, calculated by the integral of discharge curves (C-V, Fig. 10a), could achieve as high as 413 and 374 Wh kg^{-1} respectively in the 2nd and 100th cycle. The energy density retention was about 90.5% due to the little decay of capacity and voltage. Evaluated by the anode, the delivered capacity of PC-TiO₂ was about 430 $\text{mAh g}_{\text{anode}}^{-1}$, which was much higher than that of commercial graphite in half cell (about 200 mAh g^{-1}) under the similar current density.⁵⁰ With varying the current density from 100, 200, 400, 800 to 1600 mA g^{-1} , the cell could still work well with capacities of 105, 102, 95, 85 and 67 $\text{mAh g}_{\text{cathode}}^{-1}$ (Fig. 10c, d). Finally, the cell could recover back to 105 mAh g^{-1} at the current density of 100 mA g^{-1} , demonstrating the good rate capability and stability of the electrode materials.

Furthermore, the full cell of TiO₂-C (93wt%)/LiNi_{0.5}Mn_{1.5}O₄ was also investigated. Compared to the battery of PC-TiO₂/LiNi_{0.5}Mn_{1.5}O₄, an obvious work voltage platform around 2.75 V appeared. It should be ascribed to the voltage platform of TiO₂-C around 1.70 V due to the high amount of TiO₂, as shown in Fig. 11a and Fig. 7. The CE of the cell in the first cycle was 62%, and it increased fast close to an average value of 96% in the following cycles. For this cell, an average capacity of 80 $\text{mAh g}_{\text{cathode}}^{-1}$ could be delivered with a retention of 91.2% (vs. the 3rd cycle) over 100 cycles (Fig. 11b). The energy densities of the cell in the 1st and 100th cycle were about 264 and 209 Wh kg^{-1} respectively with a retention of 79%. Due to the high voltage platform and lower capacity of TiO₂-C

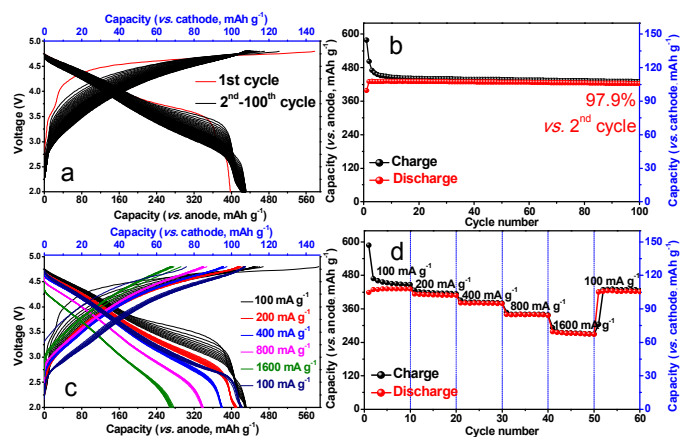


Fig. 10 (a) Charge-discharge curves, (b) cycling ability in the initial 100 cycles at 100 mA g^{-1} , (c) rate charge-discharge curves and (d) capabilities of full cell of PC-TiO₂(30wt%)/LiNi_{0.5}Mn_{1.5}O₄ under different current densities from 100-1600 mA g^{-1} .

anode, the energy density was rationally lower than that of PC-TiO₂. The delivered capacity of TiO₂-C was about 240 mAh g_{anode}⁻¹ which was similar as that of graphite, but it was still higher than most previous TiO₂-based materials in half-cell and also the safety of the cell was largely improved. In the rate test, the cell demonstrated capacities around 84, 82, 75, 60, 25 mAh g⁻¹ under the current densities of 100, 200, 400, 800, 1600 mA g⁻¹. And also, it could recover back to 83 mAh g⁻¹ at the rate of 100 mA g⁻¹. The rate performance was not as good as that of PC-TiO₂ based cell, further demonstrating that embedding TiO₂ nanocrystals into the porous carbon was good for obtaining high capacity.

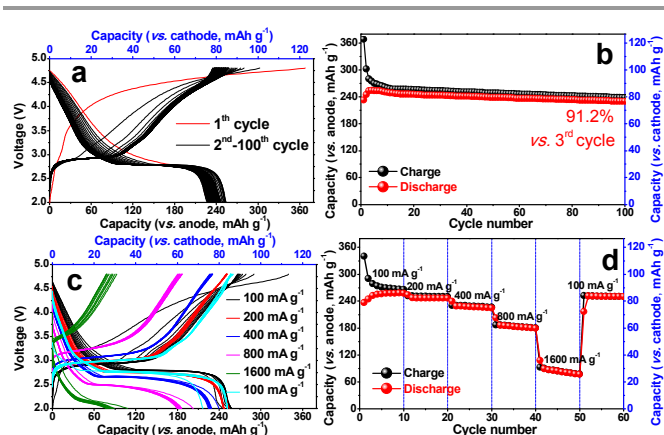


Fig. 11 (a) Charge-discharge curves, (b) cycling ability in the initial 100 cycles at 100 mA g⁻¹, (c) rate charge-discharge curves and (d) capabilities of full cell of TiO₂-C (93wt%)/LiNi_{0.5}Mn_{1.5}O₄ under different current densities from 100-1600 mA g⁻¹.

Conclusions

A new and simple strategy was developed to synthesis different kinds of TiO₂&C composite, and it could be readily extend to prepare other kind of PC-metal (oxide) just varying the precursor. Based on this strategy, a series of hierarchical PC-TiO₂ composite consisting of TiO₂ nanocrystals and porous carbon, as well as the composite of TiO₂-C were prepared readily. The high dispersion of TiO₂ nanocrystals in the porous carbon was well controlled but which was hard to be achieved before. Varying the loading of TiO₂, the lithium storage ability of composite could be finely controlled from 546 to 446 mAh g⁻¹ at the rate of 50 mA g⁻¹. Moreover, a very stable cycling performances and rate capabilities could also be obtained from 50 mA g⁻¹ to 1600 mA g⁻¹. Even for the composite of TiO₂-C (93wt%), its capacity of 352 mAh g⁻¹ at 50 mA g⁻¹ was much higher than most reported TiO₂ materials. To promote the commercialization of TiO₂-based anode, new full batteries versus LiNi_{0.5}Mn_{1.5}O₄, such as PC-TiO₂/LiNi_{0.5}Mn_{1.5}O₄ and TiO₂-C/LiNi_{0.5}Mn_{1.5}O₄, were successfully assembled and investigated for the first time. Promisingly, the battery of PC-TiO₂/LiNi_{0.5}Mn_{1.5}O₄ could deliver a high energy density of 413 Wh kg⁻¹ and also show good rate capability with an energy retention of 90.5% over 100 cycles. This is an original initial

try to applying different kinds of TiO₂-based composites in full batteries, and it could be significant to facilitate its applications in lithium and current sodium ion battery.

Acknowledgements

Financial supports from the Nature Science Foundation of China (Nos. 20873089, 20975073), Nature Science Foundation of Jiangsu Province (Nos. BK2011272), Industry-Academia Cooperation Innovation Fund Projects of Jiangsu Province (Nos. BY2011130), Key Laboratory of Lithium Ion Battery Materials of Jiangsu Province, China Scholarship Council (File. No. 201306920005) and Graduate Research and Innovation Projects in Jiangsu Province (CXZZ13_0802) are gratefully acknowledged. This work was supported by the National Research Foundation of Korea (NRF) grant funded by the Korea government (MEST) (No. 2009-0092780) and by Basic Science Research Program through the National Research Foundation of Korea (NRF) grant funded from the Ministry of Education, Science and Technology (MEST) of Korea for the Center for Next Generation Dye-sensitized Solar Cells (No. 2010-0001842).

Notes and references

^a College of Chemistry, Chemical Engineering and Materials Science, Soochow University, Suzhou 215123, P. R. China. E-mail: jwzheng@suda.edu.cn;

^b Department of Energy Engineering, Hanyang University, Seoul, 133-791, Republic of Korea; E-mail: yksun@hanyang.ac.kr; mingjun6297@gmail.com;

^c Institute of Functional Nano & Soft Materials (FUNSOM) and Jiangsu Key, Laboratory for Carbon Based Functional Materials & Devices, Soochow University, Suzhou, Jiangsu 215123, P. R. China.

†Electronic Supplementary Information (ESI) available: Comparative electrochemical performance of porous carbon, TiO₂ nanoparticles and their composite by physically mixing. See DOI: 10.1039/b000000x/.

1. H. Joo, J. Y. Park, C. K. Tsung, Y. Yamada, P.D. Yang and G.A. Somorjai, *Nat Mater.*, 2009, **8**, 126.
2. J. Ming, H. Y. Cheng, Y. C. Yu, Y. Q. Wu and F. Y. Zhao, *J. Mater. Chem.*, 2011, **21**, 6654.
3. X. W. Lou and L. A. Archer, *Adv. Mater.*, 2008, **20**, 1853.
4. Z. Y. Wang, D. Y. Luan, S. Madhavi, Y. Hu and X. W. Lou, *Energ. Environ. Sci.*, 2012, **5**, 5252.
5. J. J. Xu, D. Xu, Z. L. Wang, H. G. Wang, L. L. Zhang and X. B. Zhang, *Angew Chem. Int. Ed.*, 2013, **52**, 3887.
6. S. R. Davis, A.V. Chadwick and J.D. Wright, *J. Mater. Chem.*, 1998, **8**, 2065.
7. F. Yang, G. Li, P. Gao, X. N. Lv, X. Sun, Z. H. Liu and H. Fan, *Energ. Technol.* 2013, **1**, 581.
8. F. Han, W. C. Li, M.-R. Li and A.-H. Lu, *J. Mater. Chem.*, 2012, **22**, 9645.
9. J. Ming, J.B. Park and Y. K. Sun, *ACS Appl. Mater. Interf.*, 2013, **5**, 2133.
10. L. Yu, L. Zhang, H. Bin Wu, G.Q. Zhang and X.W. Lou, *Energ. Environ. Sci.*, 2013, **6**, 2664.

11. S. J. Ding, J. S. Chen, Z. Y. Wang, Y. L. Cheah, S. Madhavi, X. A. Hu and X. W. Lou, *J. Mater. Chem.*, 2011, **21**, 1677.
12. Z. Wang, Z.C. Wang, S. Madhavi and X. W. D. Lou, *Chem. Eur. J.*, 2012, **18**, 7561.
13. T. Lan, Y. Liu, J. Dou, Z. Hong and M. Wei, *J. Mater. Chem. A*, 2014, **2**, 1102.
14. G. Ji, D. Bing, Y. Ma, J. Y. Lee, *Energy Technol.*, 2013, **2**, 567.
15. J. Ming, H. Ming, W. J. Kwak, C. Shin, J. Zheng and Y. K. Sun, *Chem Commun*, 2014, DOI: 10.1039/c4cc02657h.
16. G. Armstrong, A. R. Armstrong, P. G. Bruce, P. Reale and B. Scrosati, *Adv. Mater.*, 2006, **18**, 2597.
17. A. R. Armstrong, G. Armstrong, J. Canales, R. Garcia and P.G. Bruce, *Adv Mater*, 2005, **17**, 862.
18. H. Ming, Y. Yan, J. Ming, X. Li, Q. Zhou, H. Huang and J. Zheng, *Rsc Adv*, 2014, **4**, 12971.
19. Q. L. Wu, J. C. Li, R. D. Deshpande, N. Subramanian, S.E. Rankin, F. Q. Yang and Y. T. Cheng, *J. Phys. Chem. C*, 2012, **116**, 18669.
20. L. G. Xue, Z. Wei, R. S. Li, J. L. Liu, T. Huang and A. S. Yu, *J. Mater. Chem.*, 2011, **21**, 3216.
21. B.L. He, B. Dong and H.L. Li, *Electrochem Commun.*, 2007, **9**, 425.
22. J. Y. Liao, D. Higgins, G. Lui, V. Chabot, X. Xiao and Z. Chen, *Nano Lett.*, 2013, **13**, 5467.
23. Y. Luo, J. Luo, J. Jiang, W. Zhou, H. Yang, X. Qi, H. Zhang, H.J. Fan, D.Y.W. Yu, C.M. Li and T. Yu, *Energ. Environ. Sci.*, 2012, **5**, 6559.
24. W. Xiong, Y. D. Wang and H. Xia, *Mater. Technol.: Adv. Perform. Mater.*, 2013, **28**, 260.
25. T. Xu, J. Song, M. L. Gordin, H. Sohn, Z. Yu, S. Chen and D. Wang, *ACS Appl. Mater. Interf.*, 2013, **5**, 11355.
26. J. Sun, H. Liu, X. Chen, D.G. Evans, W. Yang and X. Duan, *Adv Mater*, 2013, **25**, 1125.
27. Y. S. Hu, L. Kienle, Y.G. Guo and J. Maier, *Adv. Mater.*, 2006, **18**, 1421.
28. H. Lindstrom, S. Sodergren, A. Solbrand, H. Rensmo, J. Hjelm, A. Hagfeldt and S. E. Lindquist, *J. Phys. Chem. B*, 1997, **101**, 7717.
29. W. Wang, Q. Sa, J. Chen, Y. Wang, H. Jung and Y. Yin, *ACS Appl. Mater. Inter.*, 2013, **5**, 6478.
30. N. D. Petkovich, S. G. Rudisill, B. E. Wilson, A. Mukherjee and A. Stein, *Inorg. Chem.*, 2014, **53**, 1100.
31. T. Berger, D. Monllor-Satoca1, M. Jankulovska, T. Lana-Villarreal and R. Gómezl, *ChemPhyChem*, 2012, **13**, 2824.
32. J. Lee, Y. S. Jung, S. C. Warren, M. Kamperman, S. M. Oh, F. J. DiSalvo and U. Wiesner, *Macromolecular Chem. Phys.*, 2011, **212**, 383.
33. Z. Ren, C. Chen, X. Fu, J. Wang, C. Fan, G. Qian and Z. Wang, *Mater. Lett.*, 2014, **117**, 124.
34. Z. H. Wen, S. Q. Ci, S. Mao, S. M. Cui, Z. He and J. H. Chen, *Nanoscale Res Lett*, 2013, **8**, 499.
35. L. Liu, Q. Fan, C. Sun, X. Gu, H. Li, F. Gao, Y. Chen and L. Dong, *J Power Sources*, 2013, **221**, 141.
36. J. Zhang, X. Yan, J. Zhang, W. Cai, Z. Wu and Z. Zhang, *J Power Sources*, 2012, **198**, 223.
37. J. Liu, S.Z. Qiao, H. Liu, J. Chen, A. Orpe, D. Zhao and G.Q. Lu, *Angew. Chem. Int. Ed.*, 2011, **50**, 5947.
38. J. Ming, W. J. Kwak, S. J. Youn, H. Ming, J. Hassoun, Y. K. Sun, *Energy Technol.*, 2014, DOI Number 10.1002/ente.201402031.
39. J. Ming, Y. Wu, L. Y. Wang, Y. C. Yu and F. Y. Zhao, *J. Mater. Chem.*, 2011, **21**, 17776.
40. J. Ming, Y. Wu, J. B. Park, J. K. Lee, F. Zhao and Y. K. Sun, *Nanoscale*, 2013, **5**, 10390.
41. K. S. W. Sing, D. H. Everett, R. A. W. Haul, L. Moscou, R. A. Pierotti and J. Rouquerol, *Pure Appl. Chem.*, 1985, **57**, 603.
42. Y. Xu, E. Memarzadeh Lotfabad, H. Wang, B. Farbod, Z. Xu, A. Kohandehghan and D. Mitlin, *Chem. Commun.*, 2013, **49**, 8973.
43. J. Ming, Y. Wu, S. Nagarajan, D. J. Lee, Y. K. Sun and F. Zhao, *J. Mater. Chem.*, 2012, **22**, 22135.
44. S. W. Liu, J. G. Yu and M. Jaroniec, *Chem. Mater.*, 2011, **23**, 4085.
45. Z. Wang, Y. Zhang, T. Xia, J. Murowchick, G. Liu and X. Chen, *Energy Technol.*, 2014, **2**, 376.
46. J. Ming, W. J. Kwak, J. B. Park, C. D. Shin, J. Lu, L. Curtiss, K. Amine and Y. K. Sun, *ChemPhysChem*, 2014, DOI: 10.1002/cphc.201400054.
47. M.G. X. Fan, J. Rong, Y. Che, N. Aroonyadet, X. Wang, Y. Liu, A. Zhang, C. Zhou, *Energy Technology*, 2014, **2**, 159-165.
48. K. V. Sreelakshmi, S. Sasi, A. Balakrishnan, N. Sivakumar, A. Sreekumar Nair, Shantikumar V. Nair and K. R. V. Subramanian, *Energy Technol.*, 2014, **2**, 257.
49. H. G. Jung, M. W. Jang, J. Hassoun, Y. K. Sun and B. Scrosati, *Nat. Commun.*, 2011, **2**, 516.
50. C. Arbizzani, F. De Giorgio, L. Porcarelli, M. Mastragostino, V. Khomenko, V. Barsukov, D. Bresser and S. Passerini, *J. Power Sources*, 2013, **238**, 17.